The effect of Pd ensemble structure on the O 2 dissociation and CO oxidation mechanisms on Au-Pd(100) surface alloys

Ismail-Can Oğuz, Tzonka Mineva, Hazar Guesmi

The effect of Pd ensemble structure on the O_2 dissociation and CO oxidation mechanisms on Au—Pd(100) surface alloys

Ismail-Can Oğuz, Tzonka Mineva, and Hazar Guesmi

Citation: The Journal of Chemical Physics **148**, 024701 (2018);
View online: https://doi.org/10.1063/1.5007247
View Table of Contents: http://aip.scitation.org/toc/jcp/148/2
Published by the American Institute of Physics

The effect of Pd ensemble structure on the O_2 dissociation and CO oxidation mechanisms on Au—Pd(100) surface alloys

Ismail-Can Oğuz, Tzonka Mineva,[a] and Hazar Guesmi[a]
Institut Charles Gerhardt Montpellier, CNRS/ENSCM/UM, 240, Avenue du Professeur Emile Jeanbrau, 34090 Montpellier, France

(Received 1 October 2017; accepted 22 December 2017; published online 11 January 2018)

The reactivity of various Pd ensembles on the Au—Pd(100) alloy catalyst toward CO oxidation was investigated by using density functional theory (DFT). This study was prompted by the search for efficient catalysts operating at low temperature for the CO oxidation reaction that is of primary environmental importance. To this aim, we considered Pd modified Au(100) surfaces including Pd monomers, Pd dimers, second neighboring Pd atoms, and Pd chains in a comparative study of the minimum energy reaction pathways. The effect of dispersion interactions was included in the calculations of the O_2 dissociation reaction pathway by using the DFT-D3 scheme. The addition of the dispersion interaction strongly improves the adsorption ability of O_2 on the Au—Pd surface but does not affect the activation energy barriers of the Transitions States (TSs). As for O_2 to dissociate, it is imperative that the TS has lower activation energy than the O_2 desorption energy. DFT-D3 is found to favor, in some cases, O_2 dissociation on configurations being identified from uncorrected DFT calculations as inactive. This is the case of the second neighboring Pd configuration for which uncorrected DFT predicts positive Gibbs free energy (ΔG) of the O_2 adsorption, therefore an endergonic reaction. With the addition of D3 correction, ΔG becomes negative that reveals a spontaneous O_2 adsorption. Among the investigated Au—Pd (100) ensembles, the Pd chain dissociates most easily O_2 and highly stabilizes the dissociated O atoms; however, it has an inferior reactivity toward CO oxidation and CO_2 formation. Indeed, CO strongly adsorbs on the palladium bridge sites and therefore poisoning the surface Pd chain. By contrast, the second neighboring Pd configuration that shows somewhat lower ability to dissociate O_2 turns out to be more reactive in the CO_2 formation step. These results evidence the complex effect of Pd ensembles on the CO oxidation reaction. Associative CO oxidation proceeds with high energy barriers on all the considered Pd ensembles and should be excluded, in agreement with experimental observations. *Published by AIP Publishing.* https://doi.org/10.1063/1.5007247

I. INTRODUCTION

Bimetallic alloys and nanoparticles have attracted considerable attention in the field of heterogeneous catalysis due to their unusually increased activity and selectivity compared to their monometallic state.[1] Their enhanced catalytic reactivity can be attributed to the synergetic effects of mixed composition metals presented as ligand (the electronic impact due to the change in the electronic density) and ensemble or lattice-strain (the geometric impact due to a different ratio of the active metal site) effects.[2,3] For example, Suo *et al.* have made use of the ensemble effect of Co to design an effective Pd—Co alloy catalyst for oxygen reduction reactions.[4] The coinage metals (Cu, Ag, Au) electronically influence the Pd catalyst by improving its selectivity in the hydrogenation reaction of acetylene.[5–7]

In recent years, the Au—Pd system demonstrates growing attention because of the possible synergy of the two Au and Pd components in low-temperature CO oxidation reactions[8,9] which is a hot topic due to concern for the environment. Monometallic Au particles are known to adsorb CO at low T (≤RT); however, they do not activate dioxygen since no oxidation is observed between molecular CO and molecular O_2 on these surfaces.[10–12] In fact, no study has reported any significant O_2 activation or dissociation to form oxygen adatoms on Au substrates, including stepped or polycrystalline surfaces between 200 and 500 K.[13] For supported catalysts, as Au cannot dissociate O_2, the activation of O_2 is predicted to occur on the oxide support (at the Au-oxide interface) when it is reducible as TiO_2[14] or CeO_2.[15] In the case of non-reducible supports such as alumina, activation of O_2 is predicted to take place on the Au nanoparticles themselves through the formation of hydroperoxo species (OOH) which could occur in the presence of water traces.[16] This suggests then that the addition of a second element to Au, able to dissociate O_2, might facilitate the CO oxidation, whatever the nature of the used oxide support.[17] Since Pd surfaces are known to dissociate O_2 at temperatures below ~100 K,[18] the idea to add Pd to Au to favor the dissociation of O_2 is prone in the literature to improve the catalytic properties of Au. Based on this thought, Goodman and co-workers have studied two types of Au—Pd model catalysts, synthesized as thin films on Mo(110) or as nanoparticles on a TiO_2 thin film.[8,9] At low pressures of CO (1×10^{-7} Torr), the observed inactivity of the catalysts in CO oxidation reactions was attributed to the formation of isolated Pd

[a]Author to whom correspondence should be addressed: hazar.guesmi@enscm.fr and tzonka.mineva@enscm.fr

sites that were incapable to dissociate O_2. At higher CO pressures, the Au—Pd alloys showed superior reactivity toward CO oxidation reactions compared with pure Pd catalysts (no comparison was made with Au). The authors concluded that Pd segregation into the surface under high CO pressure exposure leads to the formation of contiguous Pd sites, at least Pd dimers able to dissociate O_2. These experiments coupled with Infra Red Absorption Spectroscopy (IRAS) studies showed that only contiguous Pd sites, attested by the formation of bridge CO (1970-1990 cm^{-1}), could dissociate O_2 and therefore favor the CO oxidation reaction. Note that the segregation of Pd to the surface takes place under CO pressure >0.1 Torr.

In the last years, the segregation of Pd in the Au—Pd surface exposed to reactive gas such as NO, O_2, and CO was thoroughly studied by our group.[19–22] In order to understand the surface segregation phenomena of Pd in the Au—Pd(100) surface, Monte Carlo simulations based on the density functional theory (DFT)-Ising model[23,24] were performed for different temperatures and CO pressures.[20] The resulted segregation isotherms confirmed the Pd surface enrichment observed by previous experimental studies[8,9,22] and evidenced the formation of an exotic ordered structure with Pd chains on the surface. Such a stable structure is in line with the formation of Pd dimers suggested by Goodman's group.[8,9] Could this structure be responsible for the observed high performance of the Au—Pd(100) surface toward the CO oxidation reaction? This is one of the questions addressed in the present paper.

Reactive molecular beam scattering (RMBS), reflection–absorption infrared spectroscopy (RAIRS), temperature-programmed desorption (TPD), and density functional theory (DFT) techniques were used by Mullins and co-workers[25] in an attempt to enhance the fundamental understanding of oxygen activation and reaction with CO on the Pd—Au(111) surface. The results show that larger Pd ensembles favor dissociative CO oxidation, whereas associative CO oxidation and O_2 desorption are the two main competing processes for the Pd—Au surface containing small Pd ensembles. The experimental observations exclude the associative CO oxidation pathway and mechanistic insights into the interaction of oxygen are still needed.

The herein DFT work aims to investigate the reactivity of different Pd ensembles toward the O_2 dissociation and CO oxidation reactions. For this, the reactivity of pure Au(100) and Pd modified Au(100) surfaces (Pd monomers, Pd dimers, second neighboring Pd atoms, and Pd chains) are compared. The present paper is organized as follows: the computational methods are described in detail in Sec. II, and the results are presented and discussed in Sec. III. Section III starts by a deep analysis of O_2 adsorption and dissociation mechanisms with the identification of transition state (TS) barriers. Besides, the effect of adding an empirical dispersion correction to O_2 adsorption and activation processes on the different considered surfaces is analyzed. In the second part of the paper, the overall CO oxidation reaction was studied considering the Langmuir-Hinshelwood model. Two CO oxidation reaction mechanisms are analyzed. In the first one, CO_2 formation occurs after dissociated oxygen interacts with adsorbed CO molecules. In the second mechanism, the formation of the CO—OO intermediate was considered. Finally Sec. IV presents a brief discussion and summarizes the most important conclusions.

II. CATALYST SURFACE MODELS AND COMPUTATIONAL DETAILS

Spin unrestricted calculations were performed within the plane-wave pseudopotential method based on density functional theory as implemented in the Vienna *Ab initio* Simulation Package (VASP).[26,27] Ions are described by employing the Projector Augmented Wave (PAW)[28,29] pseudopotential for the atomic core region. The exchange–correlation energy was calculated within the Perdew, Burke, and Ernzerhof formulation of the generalized-gradient approximation (GGA-PBE).[30,31] After the extensive test calculations for the total energy convergence, the kinetic energy cutoff for plane wave expansion was set to 415 eV. Pure metallic Au(100) and alloyed Au—Pd(100) surfaces were constructed using slabs of six atomic layers representing $c(2 \times 2)$ supercells containing 48 atoms. The alloyed surfaces represent different Pd ensembles where one, two, and a chain of Pd atoms are substituted on the Au surface (see Fig. 1). Each slab was separated from its periodic images by 15 Å of vacuum space. The calculations were performed allowing relaxation of the upper four metallic layers and reactive gas molecules. The bottom two layers were fixed at the Au bulk geometry, with the calculated equilibrium lattice constants of 4.17 Å, in good agreement with the experimental value of 4.08 Å.[32] Adsorbed reactive gas was located on one side of each slab. The Brillouin zone (BZ) is sampled with a k-mesh of $5 \times 5 \times 1$ within the Monkhorst–Pack scheme. The total energy calculations are also repeated with a k-mesh $7 \times 7 \times 1$ and the difference between the values are found lower than 10^{-3} eV/atom. The convergence criterion for the electronic self-consistent cycle was fixed to 10^{-6} eV per supercell. Atomic positions and lattice parameters were both relaxed using the conjugate gradient algorithm until all the forces are below 0.01 eV $Å^{-1}$. The electronic structure of the adsorption systems was analyzed through the Bader charge density analysis[33] with the implementation of Henkelman and co-workers[34] which allows analyzing the density issued from the VASP code.

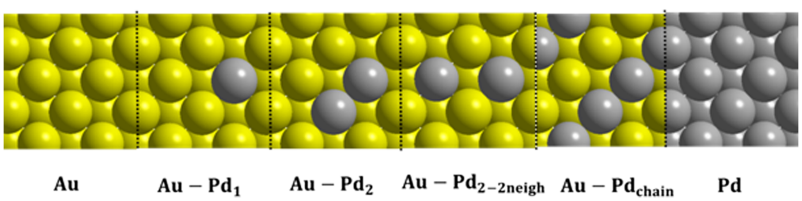

FIG. 1. (100) surfaces of pure Au, Pd substituted Au surfaces, and pure Pd. The color code is as follows: yellow for Au and gray for Pd.

The transition states (TSs) of the elementary steps were determined using the nudged-elastic-band (NEB) method.[35] Reaction pathways were optimized with a set of eight intermediate geometries (16 in complex cases), obtained by linear interpolation with a mixed internal and Cartesian coordinate system using the string theory,[36] as implemented in the Opt'n Path suite.[37] The obtained approximate transition states were refined by minimizing the residual forces below 10^{-2} eV·Å^{-1} with the quasi-Newton algorithm implemented in the VASP. All potential energy surface (PES) extrema were verified by the calculation of the vibrational frequencies within the harmonic approximation (one imaginary frequency for the transition state and none for the minimum energy structure). The Hessian or force constant matrix was computed by finite differences on nuclei forces followed by a diagonalization procedure. The resulting eigenvalues correspond to the harmonic frequencies.

From a theoretical point of view, uncorrected DFT cannot accurately capture weak interactions such as van der Waals forces and it is always difficult to ascertain the existence of a physisorbed O_2 state on the Au surfaces. In order to evaluate the effect of the dispersion correction term in the DFT calculated adsorption energies of the O_2 molecule and on the overall O_2 dissociation reaction mechanism, we employed the D3 dispersion term as implemented in the VASP code.[38] In this method, dispersion correction is added via the inclusion of pairwise atom interaction and the three-body term. Apart from DFT-D2, this method is less empirical since coefficient parameters (C_6^{ij}, C_8^{ij}) are computed from first principles calculations and these parameters are geometry (coordination number) dependent.[38] Besides, DFT-D3 is generally invoked to calculate the dispersion correction on the adsorption of small molecules on the metal surface since it is considered as more accurate due to the inclusion of the three-body term.[39,40]

III. RESULTS AND DISCUSSION

In this section, the optimized structures and calculated energies of reactants, TSs, and products of the O_2 dissociation and CO_2 formation reactions occurring on different diluted Pd ensembles of the Au—Pd(100) surface are presented and discussed. In these ensembles, Pd atoms are substituted on the Au(100) surface and denominated as follows: 1Pd monomer (Au—Pd_1), 2Pd dimer (Au—Pd_2), 2Pd second neighboring (Au—$Pd_{2\text{-}2neigh}$), and 1Pd chain (Au—Pd_{chain}). For comparison, the elementary reaction steps are also computed on monometallic Au(100) and Pd(100) surfaces. Note that each considered Pd ensemble has a given probability to exist over the surface before or during gas exposure and therefore to participate in the reaction. In a work devoted to the investigation of the ordering of Pd on Au—Pd surfaces, Gotsis *et al.* have[41] confirmed that the Pd atoms tend to be surrounded by Au atoms as first neighbors and that Pd second neighbors may exist. As an example, diluted Pd monomers on the Au(111) surface have been shown to catalyze the dissociative adsorption of H_2 at a temperature as low as 85 K.[42] Our recent studies have also demonstrated the stability of Pd monomers, dimers,[22] and Pd chains[20] in Au—Pd surface alloys interacting with reactive gas. Furthermore, the considered configurations do not include larger Pd ensembles because as demonstrated by Kim and Henkelman[43] the catalytic reactivity of Pd motifs that are larger than Pd4 on the CO oxidation tends to converge to the reactivity of the pure Pd(100) surface.

Concerning the calculation level of theory, and in order to evaluate the effect of dispersion energies, the O_2 adsorption and dissociation are computed with and without the inclusion of dispersion correction. Thus, the effect of dispersion on the adsorption and activation energy values as well as on the geometric parameters is evaluated. Finally, the activation energies and reaction paths of CO_2 formation are compared and discussed. The adsorption energies of CO and O_2 molecules calculated on pure and alloyed surfaces were calculated from the following equation:

$$E_{ads}(0\ \mathrm{K}) = E_{gas/surf} - (E_{surf} + E_{free-gas}), \qquad (1)$$

where E_{surf} represents the electronic energy of the bare surface, $E_{free\text{-}gas}$ is the electronic energy of the reactive gas, and $E_{gas/surf}$ is the electronic energy of the adsorbed system. ΔE_{ads} and $\Delta\nu_{O-O}$ are the adsorption energy and frequency differences between the DFT-D3 and DFT calculations, respectively. For O_2 in the gas phase, the triplet state was considered.

A. Adsorption and dissociation of O_2: Dispersion correction and Pd ensemble effects

1. *Adsorption of O_2*

Based on previous studies,[44] three main positions for adsorbed O_2 on (100) surfaces are possible: top-bridge-top (t-b-t), end-on (eo), and 4-fold-hollow sites (see Fig. 2). In the t-b-t configuration, both O atoms are close to the top sites while the center of mass is placed at the bridge site. In the eo configuration, one of the O atoms is on top of the metal atom and the other does not bind to the surface. This adsorption site is also called the Pauling mode. In the 4-fold-hollow site, the O_2 molecule is in the center of the four metal atoms, parallel to the surface. From the three types of oxygen adsorbates on the (100) surface, the Pauling adsorption mode (eo) is found to be less stable and not taken into consideration in this paper.

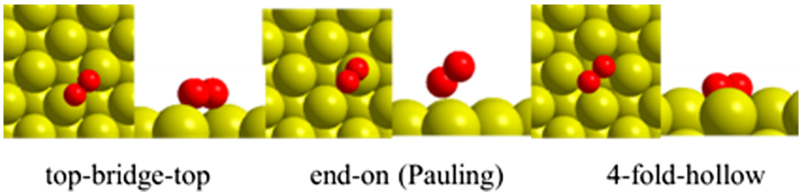

FIG. 2. Top and side views for the three main positions of adsorbed O_2 on (100) surfaces. Oxygen is represented by red balls.

TABLE I. DFT and DFT-D3 adsorption energies (E_{ads}), preferred adsorption site, O—O stretching frequencies (ν_{O-O}), and the characteristic interatomic distances (d). The computed DFT $\Delta\nu_{O-O}$ of O_2 in the gas phase is 1690 cm^{-1}.

Computational method	E_{ads} (eV)	Preferred adsorption site	ν_{O-O} (cm^{-1})	$d_{(M-O)}$ (Å)	$d_{(O-O)}$ (Å)
		Au(100)			
DFT	−0.05	4-fold	786	2.31	1.41
DFT-D3	−0.36	4-fold	776	2.30	1.41
		Au—Pd_1			
DFT	−0.23	4-fold	778	2.30[a]-2.16[b]	1.41
DFT-D3	−0.52	4-fold	766	2.30[a]-2.16[b]	1.41
		Au—Pd_2			
DFT	−0.60 (−0.55)	t-b-t (4-fold)	1035	2.04	1.33
DFT-D3	−0.82 (−0.82)	t-b-t (4-fold)	1030	2.04	1.33
		Au—$Pd_{2\text{-}2neigh}$			
DFT	−0.37	4-fold	760	2.30[a]-2.17[b]	1.41
DFT-D3	−0.64	4-fold	753	2.30[a]-2.18[b]	1.41
		Au—Pd_{chain}			
DFT	−0.71 (−0.66)	t-b-t (4-fold)	1026	2.02	1.33
DFT-D3	−0.93 (−0.93)	t-b-t (4-fold)	1024	2.02	1.33
		Pd (100)			
DFT	−1.50	4-fold	700	2.11	1.42
DFT-D3	−1.72	4-fold	692	2.11	1.42

[a]Au—O.
[b]Pd—O.

Energetic, geometric, and frequency calculations of the O_2 molecule adsorbed on the different considered Au—Pd surfaces are depicted in Table I. The preferred adsorption configurations are shown in Fig. 3 (denominated "initial").

From DFT optimized calculations and as expected, the adsorption energies are found to be very weak on the Au surface (−0.05 eV) and are found to increase with increasing Pd assemblies on the surface. Over monometallic Pd, the adsorption energy is predicted to be −1.5 eV, in line with previous theoretical results.[45] Adding the empirical dispersion (D3) interactions improve the adsorption ability of O_2 on Au(100) with an adsorption energy change ΔE_{ads} = −0.31 eV. The D3 corrections lead to less pronounced stabilization of the adsorbed O_2 in the presence of one Pd (Au—Pd_1) monomer and two Pd (Au—$Pd_{2\text{-}2neigh}$) monomers with ΔEads = −0.29 and −0.27 eV, respectively. The dispersion interactions have a least impact on Pd dimers, chains, and monometallic Pd surfaces (ΔEads = −0.22) as follows from the results in Table I. Considering the entropic contribution to the Gibbs free energy of O_2 desorption, at the conventional operating temperature of CO oxidation, which is of −0.64 eV at 298 K and 1 bar,[46,47] the uncorrected DFT calculated O_2 adsorption energies on Au(100), Au—Pd_1(100), Au—$Pd_{2\text{-}2neigh}$(100), and Au—Pd_{chain} surfaces lead to positive Gibbs free energies ΔG ($\Delta G = E_{ads}(DFT) - T\Delta S_{O2}$ with $-T\Delta S_{O2}$ = +0.64 eV.[45,46] This means that the O_2 molecule adsorbed on the monometallic Au surface, the isolated Pd monomers, the Pd second neighboring atoms, and even on the Pd dimers has a higher probability to desorb than to adsorb. Surprisingly, when the D3 dispersion-like term is added, the latter conclusion remains valid only for the pure Au and the isolated Pd monomers, which is in high agreement with experimental observations.[25] Indeed, for the case of Au—$Pd_{2\text{-}2neigh}$(100), Au—Pd_2(100), and Au—Pd_{chain}(100), the calculated O_2 adsorption energies ≤−0.64 eV predict zero or negative Gibbs free energies. This result suggests that the inclusion of dispersion correction may favor O_2 adsorption on configurations (Pd second neighboring atoms and Pd dimers) that would otherwise be identified as inactive.

Concerning the preferable adsorption site of O_2 molecule, dispersion correction seems to play a role only for the case of Au—Pd surfaces with Pd dimers and chains. More precisely, both DFT and DFT-D3 calculations predict the 4-fold site to be a solely preferred site over the (100) monometallic Au and Pd surfaces as well as on Au—Pd_1 and Au—$Pd_{2\text{-}2neigh}$ surfaces. For Au—Pd_2(100) and Au—Pd_{chain}(100), two preferred adsorption sites, the t-b-t site (where each oxygen interacts with one Pd) and the 4-fold site, are predicted. The DFT adsorption energy difference of +0.05 eV is found between

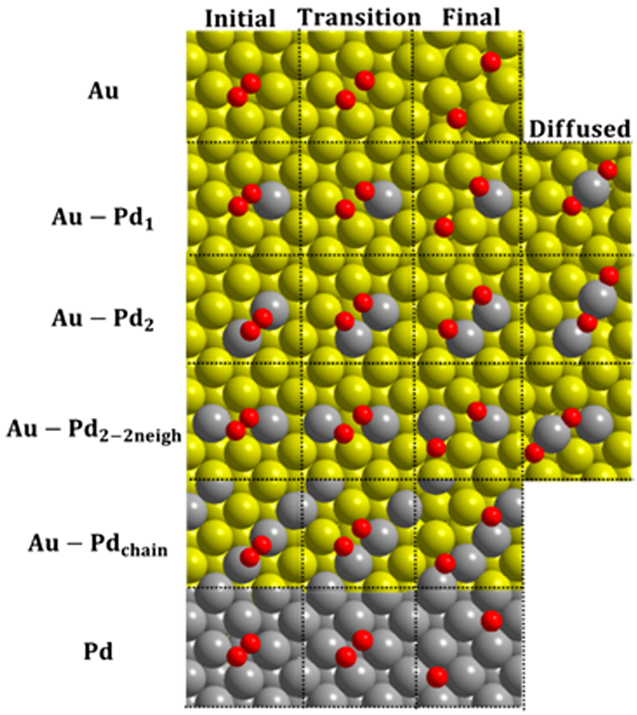

FIG. 3. The structures of O_2 preferred adsorption (initial), transition, and dissociated (final) states. The lowest energy structures obtained from atomic oxygen surface diffusion (diffused) are also shown.

t-b-t and 4-fold sites, with a preference to the t-b-t one. The dispersion correction cancels this energy difference giving E_{ads}(t-b-t) = E_{ads}(4-fold) (see Table I). Let us note that the t-b-t O_2 adsorption on the Au—Pd_{chain}, which represents 1/2 monolayer Pd coverage of the Au(100) surface, is predicted to be more favored by 0.1 eV than that on the Pd dimer (Au—Pd_2). This result indicates that there could be some effect of unsaturated Pd atoms in the chain on the O_2 adsorption energy in comparison to the Au—Pd_2 configuration.

The O_2 adsorption causes a significant O—O bond elongation in all the cases, compared to the O—O distance in the gas phase that is 1.23 Å using DFT. The O—O bond of adsorbed O_2 on dimers and chains of Pd is 0.1 Å shorter than that in O_2 adsorbed on the monometallic Au and Pd surfaces as well as on the diluted Au—Pd surfaces. Indeed, it appears that the O—O distance depends only on the adsorption site (shorter on t-b-t sites and longer on 4-fold sites). As expected, the energy gain of the order of 0.2–0.3 eV due to the attractive dispersion corrections is too small and does not cause any noticeable shortening in the interatomic distances, in agreement with previous theoretical results.[48]

The vibrational frequency of adsorbed O_2 and metal-O_2 is also related to the type of adsorption site. The O—O distance elongations correlate well with the obtained red shifts of O—O stretching frequencies in respect of those computed by us, ν_{O-O} = 1690 cm^{-1} for the gas-phase O_2. In the t-b-t bonding on Au—Pd_2 and Au—Pd_{chain} surfaces, the red shift ($\Delta\nu_{O-O}$) is ~690 cm^{-1}. In the 4-fold sites, an oxygen molecule undergoes a stronger deformation and $\Delta\nu_{O-O}$ amounts to 900-1000 cm^{-1}. Experimentally, O_2 molecular adsorption on Pd(100) is documented to occur at T = 80 K. The O—O stretching frequency obtained from High Resolution Electron Energy Loss Spectroscopy (HREELS) is 90 meV (726 cm^{-1})[17] which reveals a very good agreement with our computed ν_{O-O} frequency in the 4-fold O_2 on Pd(100). It is commonly accepted that the very large red shift of the O—O stretching frequencies in molecularly adsorbed oxygen on open and closed packed 4d-metallic surfaces measured since earlier HREELS studies[17] originates from the formation of peroxo and/or superoxo dioxygen species. The elongation and by consequence the weakening of the O—O bond are associated with an electron transfer from the surface to the unoccupied O_2 orbital. The Bader charges that we computed for the six adsorbate structures corroborate this understanding. The charge of t-b-t adsorbed O_2 is less negative (q_{O_2} = −0.5) than that of 4-fold hollow adsorbed O_2 (q_{O_2} = −0.8) in agreement with previous DFT studies of O_2 molecular adsorption on AuM (M = Ni, Pd, Pt) (111) alloy surfaces,[49] on the Au(100) surface,[44] and on Pd monomers on Au(100).[50] The Bader charges are reported in the supplementary material, Table S1.

2. Activation energy for O_2 dissociation

The dissociation of adsorbed O_2 passes through a transition state (TS), whose energy depends on the particular Pd configuration as follows from the computed activation energies in Table II. Figure 3 shows the initial state, TS, and final state configurations of O_2 adsorption and dissociation reactions on the six considered surfaces.

The activation energy barriers collected in Table II are found to vary between +0.09 and +0.63 eV, depending on the (100) surface composition and Pd arrangements. The very low energy value calculated on the monometallic Pd surface (+0.09 eV) agrees very well with the experimental results demonstrating that the O_2 dissociation on the bare Pd(100) surface precedes the associative adsorption at a temperature as low as T = 10 K.[17] At an elevated temperature (T = 150 K), molecularly adsorbed oxygen is detected only when the entire surface is covered with atomic oxygen and the adsorption of O_2 is also readily followed by a spontaneous dissociation.[51] Although the DFT (0 K) calculated O_2 adsorption on Pd(100) is rather strong (E_{ads} = −1.50 eV with DFT and E_{ads}

TABLE II. Activation energies (E_{act}), interatomic distances of O_2 in the transition state on the O_2 dissociation pathways, and the activation energy differences (ΔE_{act}) between DFT and dispersion corrected DFT-D3 calculations.

	DFT		DFT-D3		
Surface	E_{act} (eV)	$d_{(O-O)}$ (Å)	E_{act} (eV)	$d_{(O-O)}$ (Å)	ΔE_{act} (eV)
Au(100)	0.63	2.06	0.59	2.06	0.04
Au—Pd_1(100)	0.54	2.04	0.51	2.04	0.03
Au—Pd_2(100)	0.56(0.50)[a]	2.04	0.47	2.03	0.09(0.03)[a]
Au—$Pd_{2\text{-}2neigh}$(100)	0.44	2.02	0.41	2.01	0.03
Au—Pd_{chain}(100)	0.51(0.47)[a]	1.98	0.43	1.98	0.08(0.04)[a]
Pd(100)	0.09	1.70	0.09	1.70	0.00

[a]Activation energy barriers calculated by taking the 4-fold adsorption site as the initial adsorbed state.

−1.72 eV with DFT-D3), the predicted O—O distance of 1.42 Å is larger compared to the O—O distances on Au—Pd(100) surfaces (see Table I). This result shows that the molecule is close to its dissociation state. Indeed, the O—O distances in the TS on the bare Pd surface is 1.70 Å, that is, 0.28 Å longer compared to d(O—O) in molecularly adsorbed O_2 (see Table I).

Comparing the DFT adsorption energies in Table I with the TS barriers in Table II, we note that the O_2 molecule will preferably desorb from Au(100) and Au—$Pd_{2\text{-}2neigh}$ because of the larger activation barriers than the respective adsorption energies. When the D3 dispersion-like term is added, this conclusion remains valid only for the pure Au(100) surface but changes in the case of Au—$Pd_{2\text{-}2neigh}$(100). In the latter case, the O_2 desorption energy, that is, the negative of E_{ads} (DFT-D3), is +0.64 eV, being now larger than the DFT-D3 TS barrier energy of +0.41 eV. The latter result reasonably agrees with Eact = +0.33 eV, reported in the previous theoretical work on O_2 dissociation on second neighboring Pd atoms in AuPd(100).[50] We found similar activation energies in the case of Au—Pd_2(100) (Eact = +0.47 eV) and Au—Pd_{chain}(100) (Eact = +0.43 eV) surfaces, using the DFT-D3. This can be explained by the geometry of the TS complexes. As follows from the inspection of all the TS structures, the O—O bond breaking processes only occur over the 4-fold sites of the (100) surface. Because the favorable adsorption site of O_2 on Au—Pd_2 and Au—Pd_{chain} is the t-b-t one, the TS structures on these surfaces undergo structural changes in comparison to the respective initial states (see Fig. 3). These changes are because of the diffusion of the O_2 molecules from the preferred t-b-t adsorption site to the 4-fold site in the TS structures. The examination of the structural transition from the t-b-t to the 4-fold adsorption sites show that in the absence of D3 correction, O_2 has to overcome an energy barrier of +0.05 eV to diffuse from the t-b-t to 4-fold site. This result also suggests that different conclusions can be made if dispersion corrections are not considered and in particular for the initial state and TS that involve different Au and Pd atoms. Because the dispersion interactions can affect the rate limiting step of reactions over Au-Pd surfaces, all the results that are presented in the following include the D3 correction.

3. O_2 dissociation

In Fig. 4, a superposition of the O_2 dissociation reaction pathways on the six considered surfaces is presented for comparison. The endothermic O_2 dissociation (the energy of the adsorbed O atoms is higher than that of the adsorbed O_2 molecule) on Au—Pd_1(100), Au—Pd_2(100), and Au—$Pd_{2\text{-}2neigh}$(100) is evidenced (see Table III). The reaction becomes exothermic on surfaces involving Pd dimers and monomers only if atomic oxygen diffusion from Au to Pd is considered (see diffused configuration in Fig. 3). The surface geometries after the diffusion are also shown in Fig. 3 together with O adsorption sites in final and diffused configurations. The optimization calculations of surface oxygen lead to lower states than the final one in the case of Au—Pd_1, Au—Pd_2, and Au—$Pd_{2\text{-}2neigh}$. The exothermic reaction without additional O_2 displacements is established

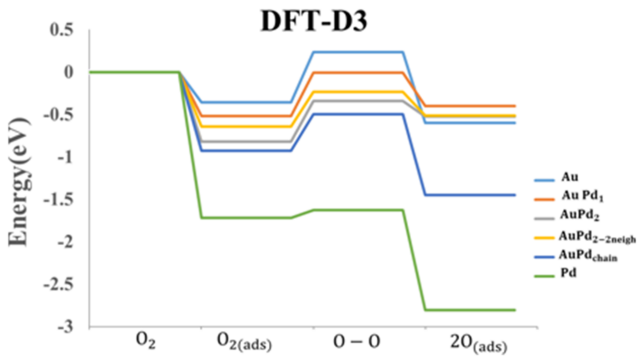

FIG. 4. Minimum energy reaction pathways for O_2 adsorption and dissociation on Au(100), Au—Pd_1(100), Au—$Pd_{2\text{-}2neigh}$(100), Au—Pd_2(100), Au—Pd_{chain}(100), and Pd(100) from DFT-D3 calculations. The energies of the initial states, TSs, and final states are calculated by taking as a reference the bare surface + O_2 in the gas phase. The corresponding energies calculated by uncorrected DFT could be found in Tables I and II.

for the O_2 dissociation on Au—Pd_{chain}(100) and Pd(100) surfaces. Among the Au—Pd surfaces studied here, the preferred Pd arrangement for the O_2 molecular adsorption, dissociation, and stabilization of the dissociated O atoms is therefore Au—Pd_{chain}(100).

Examination of the charge difference analysis and Bader charges, presented in Tables S2 and in Fig. S1 of the supplementary material, for the transition states shows a similar amount of charge transfer from the metal surface to the oxygen atoms. Pd atoms are systematically more positive than Au centers participating in the reaction. In addition, a charge accumulation is observed along the first layer Pd and the second layer Au bond (see Fig. S1 of the supplementary material). This agrees with the very detailed orbital analysis reported by Wang *et al.*[50] for the O_2 dissociation mechanism on Pd monomers dispersed on Au(100). The charge accumulations and/or depletions between the Au atoms of interest in the first and second layers are significantly smaller than those between Pd and Au, rendering the Au atom less positive. The negatively charged oxygen will be strongly attracted by the more positive Pd atom than the Au atom. Note that the charges located at O-centers are comparable on all the surfaces ranging from pure Au to pure Pd and again their amount depends on the adsorbate structure rather than on the compositions of the metal surface. This result would suggest that the O_2 dissociation reaction on Au—Pd(100) is governed by the ensemble effect.

TABLE III. Adsorption sites of dissociated oxygen atoms in the final and diffused states (see Fig. 3). Reaction energy of O_2 dissociation ($\Delta\mathbf{E_{F\text{-}I}}$) and including O diffusion step ($\Delta\mathbf{E_{D\text{-}I}}$). $\Delta\mathbf{E}$ is calculated as the differences between the final and initial states, $\Delta E_{F\text{-}I}$, and the diffused and initial states, $\Delta E_{D\text{-}I}$.

Surface model	Final state configuration	$\Delta\mathbf{E_{F\text{-}I}}$ (eV)	Diffused configuration	$\Delta\mathbf{E_{D\text{-}I}}$ (eV)
Au(100)	3-fold	−0.24	...	...
Au—Pd_1(100)	3-fold and bridge	0.12	3-fold	−0.17
Au—Pd_2(100)	Bridge	0.29	3-fold and bridge	−0.33
Au—$Pd_{2\text{-}2neigh}$(100)	3-fold and bridge	0.13	3-fold	−0.25
Au—Pd_{chain}(100)	3-fold	−0.52	...	...
Pd(100)	4-fold	−1.09	...	...

B. CO oxidation and CO_2 formation

This part of the section is devoted to the identification of CO_2 formation minimum energy reaction pathways. At a first glance at the CO oxidation overall reaction, it seems likely that the Langmuir-Hinshelwood mechanism takes place between chemisorbed CO and O species, followed by CO + O recombination and CO_2 desorption steps. This reaction mechanism, which is fully supported by experiments,[51] will be thoroughly analyzed and discussed. As will become apparent below, another mechanism, which was considered in previous theoretical studies,[51,52] involving an OOCO intermediate complex will be considered. This mechanism denoted herein as association mechanism will be discussed in the second part.

1. CO_2 formation from CO and O

As the above results show a better dissociation ability of oxygen (the lowest activation energy barriers) over Au—$Pd_{2\text{-}2neigh}$(100) and Au—Pd_{chain}(100) surfaces, the following analyses will concern only these two configurations. All the results are obtained with DFT-D3.

In Figs. 5 and 6 are presented the overall reaction pathways of CO oxidation on the two considered Pd ensembles. The successive elementary steps are as follows: O_2 molecular adsorption, O_2 dissociation, the adsorption of CO in the vicinity of one of the two adsorbed atomic oxygen, and CO_2 formation. In all cases, two adsorption sites are investigated for the adsorption of CO on the surface: CO adsorbs on Pd sites or on Au sites. For each system, the initial state (the zero reference) is taken as the sum of the energies of the considered bare surface and CO and O_2 in the gas phase. All calculated vibrational frequencies of minimum energy reaction pathways are provided in the supplementary material, Table S3.

The O_2 dissociation reaction, slightly endothermic (+0.13 eV) on Au—$Pd_{2\text{-}2neigh}$ and highly exothermic on the Pd chain (−0.52 eV), leads to dissociated oxygen atoms (O) bounded to Pd and Au sites (Figs. 5 and 6). On both configurations, the coming CO molecule has the possibility to adsorb

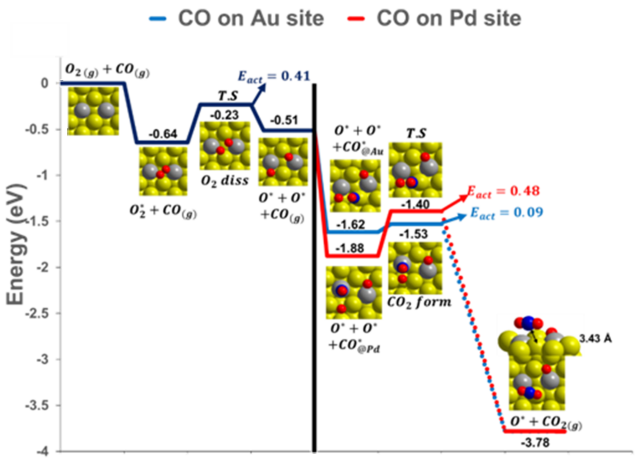

FIG. 5. Calculated energy profiles for O_2 dissociation and CO_2 formation on the Au—$Pd_{2\text{-}2neigh}$ (100) surface. (*) indicates the adsorbed state. The color code is as follows: yellow for Au, gray for Pd, red for O, and blue for C.

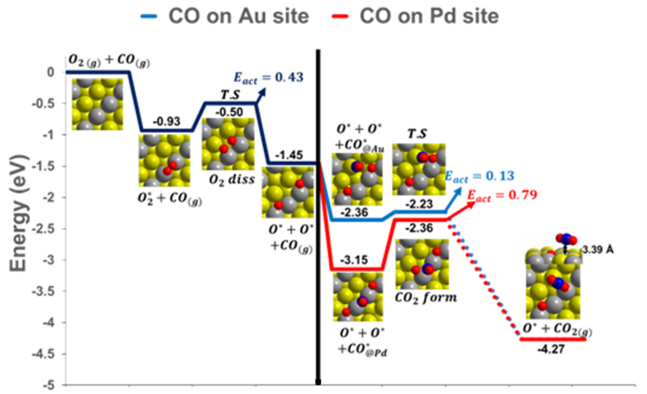

FIG. 6. Calculated energy profile for O_2 dissociation and CO_2 formation on the Pd chain and Pd_{chain}(100) surface. (*) indicates the adsorbed state.

either on Au or on Pd sites in the vicinity of dissociated oxygen. Let us note that for the case of the Au—$Pd_{2\text{-}2neigh}$ (100) surface, the diffusion of oxygen atoms (O) was not considered. Indeed, as illustrated by the configuration reported in Fig. 3, the oxygen diffusion leads to the surface reconstruction and the formation of Pd dimers. This result is consistent with previous studies evidencing the stability of contiguous Pd sites in the presence of reactive gas.[22] So, in order to compare the reactivity of isolated Pd sites by Au [present in the case of the Au—$Pd_{2\text{-}2neigh}$ (100) surface] and contiguous Pd sites, the adsorption of CO on 2nd neighboring Pd is considered before the oxygen diffusion process occurs.

From general point of view, the adsorption of CO and the CO_2 formation on Au sites (blue lines) are found to be less exothermic than on Pd sites (red lines). On both Au—Pd surfaces, CO binds through the C-atom to the metallic site in the vicinity of O.

Over the Au—$Pd_{2\text{-}2neigh}$ (100) surface (Fig. 5), CO adsorbs on the top position slightly tilted toward O. The calculated DFT-D3 adsorption energies are found to be −1.11 eV and −1.37 eV on Au and Pd sites, respectively. The values of adsorption energies are on the order of +0.28 and +0.79 eV lower than on the corresponding sites with surface free from oxygen atoms, respectively. The calculated C—O stretching frequencies are computed to be of $\nu_{C-O} = 2152\ cm^{-1}$ and $\nu_{C-O} = 2124\ cm^{-1}$ on Au and Pd sites, respectively. These DFT-D3 values are obtained after the application of a correction factor of 1.033.[20–22] In order to explore the nature of the adsorption sites for CO adsorbed on the oxygen-saturated Au—Pd(100) surface, Liu *et al.*[53] have collected a series of infrared spectra and assigned the different peak to the corresponding adsorption sites. According to that work, carbon monoxide adsorptions on top of Au and Pd sites are manifested by CO stretching frequencies at ∼2109 cm^{-1} and at ∼2087 cm^{-1}, respectively. Although our calculation overestimates these frequency values, it respects the shift of about 22 cm^{-1} between the two assigned peaks. From identified transition state, the CO oxidation reaction is found to take place with a small activation barrier of +0.09 eV on the Au site and a barrier of +0.48 eV on the Pd site. Each of these identified transition states is characterized by a unique imaginary frequency of $213i\ cm^{-1}$ and $226i\ cm^{-1}$, respectively, and the carbon atom in CO is

separated from O by ~2 Å (2.03 Å on the Au site and 2.12 Å on the Pd site).

In the case of the Au—Pd_{chain}(100) surface (Fig. 6), the coming CO molecule adsorbs differently depending on whether the site is Au or Pd. Thus, while CO adsorbs on top of the Au atom (although slightly tilted), it prefers the bridge sites over the chain of Pd. The adsorption energy of CO on the Au atom is calculated to be −0.91 eV (blue line). The distances between C and O are 2.91Å. To form CO_2, the system has to overcome a small barrier of +0.13 eV which is only +0.04 eV higher than that on the Au site of the Au—$Pd_{2\text{-}2neigh}$(100) surface. In the transition state, the formed C—O bond is found to be 1.98Å equivalent to an imaginary frequency of 225*i* cm^{-1}. Over Pd, the adsorption of CO is much more exothermic and the adsorption energy is higher by 0.79 eV than on Au. This result is in line with Temperature Programmed Desorption (TPD) results[53] where the measured peaks for CO on top of Au and on bridge of Pd atoms shift and lose intensity with increasing temperatures and desorb above 126 K and 400 K, respectively. At the Pd bridge site, the C—O stretching frequency is computed to be ν_{C-O} = 1949 cm^{-1}, which concords with the measured experimental IR values at 1973 cm^{-1}.[22,53] To form CO_2, the system has to overcome a high activation barrier of +0.79 eV with the calculated imaginary frequency of the transition state of 278*i* cm^{-1}. This high activation energy results from the strong bonding of CO on bridge Pd sites over chain configuration. Note that similar results (Fig. S2 of the supplementary material) are found for the CO adsorption and CO_2 formation pathways on Pd dimers.

Interestingly, whatever the considered Au—Pd ensemble, once O attachment to CO occurs, CO_2 forms and readily desorbs. In all the cases, the geometry optimizations of TS structures show changes from single C—O to double C=O bonds occurring simultaneously with the breaking of the C-metal bond followed by the transformation of the O=C—O group into the linear geometry of the gas phase CO_2 molecule. The final highly exothermic minimum energy states show CO_2(g) at distances higher than 3 Å from the surface. This result together with the lower identified CO_2 formation energy barriers of +0.09 eV and +0.13 eV indicate that CO oxidation is likely to occur when the coming CO is adsorbed on the Au site. That is, the more weakly the CO is adsorbed on the surface, the more easily it oxidizes. When CO adsorbs on Pd sites, it could be oxidized more easily on Au—Pd_{2neigh}(100) surfaces than on Au—Pd_{chain}(100). Moreover, our results suggest that the Au—$Pd_{2\text{-}2neigh}$ ensembles could be the operating active sites during low-temperature CO oxidation reaction while Au—Pd_2 and Au—Pd_{chain} ensembles would be poisoned by CO. It is worth noting that these results concord with the very low Pd coverage (0.2 ML) in Au—Pd(100) system that was reported to be able to catalyze the CO oxidation reaction at low temperature.[8,9]

Regarding the reactivity of pure gold and palladium surfaces, we first note that CO oxidation on the pure Au surfaces is not observed experimentally.[1–3] Gold surfaces and even Au-nanoparticles do not activate the dioxygen dissociation (*vide infra*). In the case of Pd surfaces, both oxygen and CO adsorb strongly at low temperatures with O_2 dissociative adsorption.[17,18] To overcome the strong Pd—CO and Pd—O interactions, a high temperature is required, which therefore turns the pure Pd surface to be not reactive for low-temperature CO oxidation.[54]

2. Association mechanism

The theoretical study of CO oxidation presented by Molina and Hammer[55] proposed an association mechanism for CO_2 formation on Au nanoparticles supported by the MgO(100) surface. According to these authors, adsorbed CO and O_2 molecule form a four-center metastable structure (OCOO), which readily dissociates into CO_2 and atomic O on the surface. The highly reactive sites for this reaction are edges of the particle placed near the oxide substrate. A similar mechanism for the CO oxidation reaction was proposed by Yuan and co-workers[56] who studied the catalytic activity of Pd ensembles (Pd dimers and trimers) over the Au(111) surface by DFT. The results show the high activity of Pd dimer in which a two-step reaction of CO + O_2 → OOCO → CO_2 + O occurs. In this work, the association mechanism was also investigated on all considered Au—Pd(100) surfaces. The first reaction step corresponds to CO and O_2 co-adsorption in nearest neighbor sites. In the second step, chemisorbed O_2 in a four-fold site or in a t-b-t site changes it adsorption mode to the end-on (eo) position to allow more interaction with adsorbed CO (see Fig. 7 for the case of Au—Pd_{chain}). This step is found to be highly energetic (spans more than 1 eV) on different considered Au—Pd ensembles. As shown in Fig. 7, over the transition state, a metastable intermediate OC–O—O complex is formed. Then, the O–O bond in the OC–O—O complex is stretched and the second TS is reached when the O—O bond elongates to 1.66-1.70 Å. The latter step occurs with relatively low energy barriers that vary from +0.05 to +0.13 eV depending on the Au—Pd ensemble. The final step corresponds to the desorption of the formed CO_2 molecule.

Our analysis of the CO oxidation reaction excludes the association reaction mechanism over the Au—Pd(100) surface where the rate determining step is found to be the change of adsorption configuration of molecular oxygen from t-b-t to end-on configuration in order to allow one of the two oxygen atoms interacting with the C atom of adsorbed CO. This result is explained by the fact that the end-on adsorption of O_2 on the (100) surface is not likely to occur. All previous studies supporting the association mechanism were conducted on flat (111),[57] stepped[58] surfaces or nanoparticles[55] where O_2 end-on adsorption may be favorable.

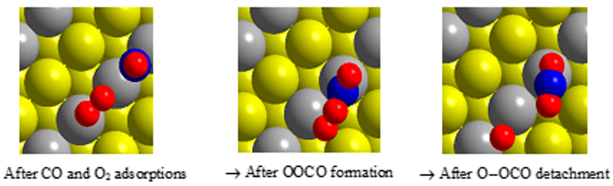

FIG. 7. Minimum energy structure configurations of CO oxidation reaction pathway occurring via an association mechanism over the Pd_{chain}(100) surface.

IV. CONCLUSIONS

In this paper, several important features are found concerning the effect of the Au—Pd ensemble on oxygen dissociation and CO oxidation reactions.

(i) Concerning the theoretical level of calculation, the inclusion of the dispersion correction term in the calculation of O_2 adsorption and dissociation reactions captures qualitative agreement with experiment that uncorrected DFT does not. Indeed, while uncorrected DFT results reveal that the O_2 molecule may preferably desorb from Au(100), Au—Pd_1(100), and Au—$Pd_{2\text{-}2neigh}$(100) because of the larger identified activation energies than adsorption energies, the O_2 dissociation is found to be favorable on Au—$Pd_{2\text{-}2neigh}$(100) when the D3 dispersion-like term is added. Similarly, while uncorrected DFT calculations predict a low adsorption energy of O_2 on Au—Pd_2(100) that leads to positive Gibbs free energy, the dispersion correction leads to more accurate results and confirms the ability of the Pd dimer ensemble to stabilize and to dissociate O_2. This result suggests that the inclusion of dispersion correction is important and may favor configurations that could not be identified by uncorrected DFT calculation

(ii) The O_2 adsorption and the subsequent dissociation reaction are energetically favorable not only on contiguous Pd sites [as in Au—Pd_2(100) and in Au—Pd_{chain}(100)] but also on the second neighboring Pd atoms. This dissociation ability is due to the Au—Pd ensemble effect. Indeed, the adsorption of O_2 on the 4-fold site of (100) surface makes it interacting with the two second neighboring Pd atoms, which deforms strongly the adsorbed O_2 molecule resulting in the O—O distance close to that in the dissociation transition state.

(iii) Minimum energy reaction pathways for CO oxidation on Au—Pd_{2chain} and on Au—$Pd_{2\text{-}2neigh}$ show very low CO_2 formation energy barriers when CO is adsorbed on Au atom and higher barriers when CO is adsorbed on Pd. This result indicates that CO oxidation is likely to occur when the coming CO is adsorbed on the Au site. In addition, because of its strong ability to absorb CO, the Pd chain configuration is found to poorly oxidize CO. By consequence, the Au—$Pd_{2\text{-}2neigh}$ ensemble may offer the best reactive Pd ensemble for low-temperature CO oxidation reactions and may explain observed experimental data. Additional investigations on the effect of the entropy as well as the diffusion of adsorbed species would provide more insights on these complex reaction mechanisms.

(iv) The CO oxidation reaction involving the formation of a metastable intermediate, the OC–O—O complex, is found to be highly energetic and this mechanism has to be excluded on the Au—Pd(100) surface.

SUPPLEMENTARY MATERIAL

See supplementary material for the Bader charge analyses (Tables S1 and S2), for the charge density differences calculated for all identified transition states of O_2 dissociation (Fig. S1), the vibration frequency values of adsorbed states and TSs of the identified reaction pathways of Figs. 5 and 6 (Table S3), and for minimum energy reaction pathways of the CO oxidation reaction on the Au—Pd_2(100) surface (Fig. S2).

ACKNOWLEDGMENTS

This work was granted access to the HPC resources of [CCRT/CINES/IDRIS] under the allocation 2017 [No. x2017087369] made by GENCI [Grand Equipement National de Calcul Intensif].

[1] R. Ferrando, J. Jellinek, and R. L. Johnston, Chem. Rev. **108**, 845–910 (2008).
[2] J. A. Rodriguez, Surf. Sci. Rep. **24**, 223–287 (1996).
[3] H. Guesmi, Gold Bull. **46**, 213–219 (2013).
[4] Y. Suo, L. Zhuang, and J. Lu, Angew. Chem., Int. Ed. **46**, 2862–2864 (2007).
[5] G. X. Pei, X. Y. Liu, X. Yang, L. Zhang, A. Wang, L. Li, H. Wang, X. Wang, and T. Zhang, ACS Catal. **7**, 1491–1500 (2017).
[6] G. X. Pei, X. Y. Liu, A. Wang, A. F. Lee, M. A. Isaacs, L. Li, X. Pan, X. Yang, X. Wang, Z. Tai, K. Wilson, and T. Zhang, ACS Catal. **5**, 3717–3725 (2015).
[7] A. J. McCue, R. T. Baker, and J. A. Anderson, Faraday Discuss. **188**, 499–523 (2016).
[8] F. Gao, Y. Wang, and D. W. Goodman, J. Am. Chem. Soc. **131**, 5734–5735 (2009).
[9] F. Gao, Y. Wang, and D. W. Goodman, J. Phys. Chem. C **114**, 4036–4043 (2010).
[10] A. G. Sault, R. J. Madix, and C. T. Campbell, Surf. Sci. **169**, 347–356 (1986).
[11] D. A. Outka and R. J. Madix, Surf. Sci. **179**, 351–360 (1987).
[12] J. Kim, E. Samano, and B. E. Koel, Surf. Sci. **600**, 4622–4632 (2006).
[13] J. Kim, E. Samano, and B. E. Koel, J. Phys. Chem. B **110**, 17512–17517 (2006).
[14] M. Valden, X. Lai, and D. W. Goodman, Science **281**, 1647–1650 (1998).
[15] C. J. Zhang, A. Michaelides, and S. J. Jenkins, Phys. Chem. Chem. Phys. **13**, 22–33 (2010).
[16] J. T. Calla and R. J. Davis, J. Phys. Chem. B **109**, 2307–2314 (2005).
[17] C. Nyberg and C. G. Tengstål, Surf. Sci. **126**, 163–169 (1983).
[18] T. Engel and G. Ertl, Adv. Catal. **28**, 1–78 (1979).
[19] M. Dhifallah, A. Dhouib, S. Aldulaijan, F. Direnzo, and H. Guesmi, J. Chem. Phys. **145**, 024701–024708 (2016).
[20] B. Zhu, J. Creuze, C. Mottet, B. Legrand, and H. Guesmi, J. Phys. Chem. C **120**, 350–359 (2016).
[21] M. Sansa, A. Dhouib, and H. Guesmi, J. Chem. Phys. **141**, 064709–064717 (2014).
[22] B. Zhu, G. Thrimurthu, L. Delannoy, C. Louis, C. Mottet, J. Creuze, B. Legrand, and H. Guesmi, J. Catal. **308**, 272–281 (2013).
[23] J. Creuze, H. Guesmi, C. Mottet, B. Zhu, and B. Legrand, Surf. Sci. **639**, 48–53 (2015).
[24] B. Zhu, H. Guesmi, J. Creuze, B. Legrand, and C. Mottet, Phys. Chem. Chem. Phys. **17**, 28129–28136 (2015).
[25] W.-Y. Yu, L. Zhang, G. M. Mullen, G. Henkelman, and C. B. Mullins, J. Phys. Chem. C **119**, 11754–11762 (2015).
[26] G. Kresse and J. Furthmüller, Comput. Mater. Sci. **6**, 15–50 (1996).
[27] G. Kresse and J. Furthmüller, Phys. Rev. B **54**, 11169–11186 (1996).
[28] P. E. Blochl, Phys. Rev. B **50**, 17953–17979 (1994).
[29] G. Kresse and D. Joubert, Phys. Rev. B **59**, 1758–1775 (1999).
[30] J. P. Perdew, K. Burke, and M. Ernzerhof, Phys. Rev. Lett. **77**, 3865–3868 (1996).
[31] J. P. Perdew, K. Burke, and M. Ernzerhof, Phys. Rev. Lett. **78**, 1396 (1997).
[32] C. Kittel, *Introduction to Solid State Physics*, 7th ed. (Wiley, New York, 1996).
[33] F. W. Bader, *Atoms in Molecules: A Quantum Theory* (Oxford Science, Oxford, UK, 1990).
[34] E. Sanville, S. D. Kenny, R. Smith, and G. Henkelman, J. Comput. Chem. **28**, 899–908 (2007).

[35]G. Henkelman, B. P. Uberuaga, and H. Jonsson, J. Chem. Phys. **113**, 9901–9904 (2000).
[36]W. E, W. Ren, and E. Vanden-Eijnden, Phys. Rev. B **66**, 052301 (2002).
[37]P. Fleurat-Lessard and P. Dayal, Code freely available at: http://perso.ens-lyon.fr/paul.fleurat-lessard/ReactionPath.html.
[38]S. Grimme, J. Antony, S. Ehrlich, and H. Krieg, J. Chem. Phys. **132**, 154104 (2010).
[39]W. Reckien, M. Eggers, and T. Bredow, Beilstein J. Org. Chem. **10**, 1775–1784 (2014).
[40]J. B. A. Davis, F. Baletto, and R. L. Johnston, J. Phys. Chem. A **119**, 9703–9709 (2015).
[41]H. J. Gotsis, I. Rivalta, E. Sicilia, and N. Russo, Chem. Phys. Lett. **468**, 162 (2009).
[42]F. R. Lucci, M. T. Darby, M. F. G. Mattera, Ch. J. Ivimey, A. J. Therrien, A. Michaelides, M. Stamatakis, and E. Ch. H. Sykes, J. Phys. Chem. Lett. **7**, 480–485 (2016).
[43]H. Y. Kim and G. Henkelman, ACS Catal. **3**, 2541–2546 (2013).
[44]M. Boronat and A. Corma, Dalton Trans. **39**, 8538–8546 (2010).
[45]D.-J. Liu and J. W. Evans, Phys. Rev. B **89**, 205406–205414 (2014).
[46]P. Atkins and J. D. Paula, *Physical Chemistry*, 8th ed. (New York, Oxford, 2006).
[47]H. Metiu, *Physical Chemistry: Statistical Mechanics*, 1st ed. (Tayler & Francis, New York, 2006).
[48]M. B. Kanoun and L. Cavallo, J. Phys. Chem. C **118**, 13707–13714 (2014).
[49]M. García-Mota and N. Lopez, Phys. Chem. Chem. Phys. **13**, 5790–5797 (2011).
[50]T. Wang, B. Li, J. Yang, H. Chen, and L. Chen, Phys. Chem. Chem. Phys. **13**, 7112–7120 (2011).
[51]M. S. Chen, D. Kumar, C. W. Yi, and D. W. Goodman, Science **310**, 291–293 (2005).
[52]T. Engel and G. Ertl, J. Chem. Phys. **69**, 1267–1281 (1978).
[53]Y. Zhou, Z. Wang, and Ch. Liu, Catal. Sci. Technol. **5**, 69–81 (2015).
[54]J. Zhang, H. Jin, M. B. Sullivan, F. Ch. H. Lim, and P. Wu, Phys. Chem. Chem. Phys. **11**, 1441–1446 (2009).
[55]L. M. Molina and B. Hammer, Phys. Rev. B **69**, 155424 (2004).
[56]D. W. Yuan, Z. R. Liu, and J. H. Chen, J. Chem. Phys. **134**, 054704 (2011).
[57]H. C. Ham, J. A. Stephens, G. S. Hwang, J. Han, S. W. Nam, and T. H. Lim, J. Phys. Chem. Lett. **3**, 566–570 (2012).
[58]A. Hussain, A. J. Muller, B. E. Nieuwenhuys, J. M. Garcia, and J. W. Niemantsverdriet, Top. Catal. **54**, 415–423 (2011).